Title

The cold-inducible RNA-binding protein RBM3 stabilises viral mRNA at cooler temperatures representative of the upper respiratory tract.

Authors

Hannah L Coutts[1*], Swathi Sukumar[1*], Hannah L Turkington[1], Stefano Bonazza[1], Emily Peate[1], Erin M P E Getty[1], Ultan F Power[1], David G Courtney[1]

** These two authors contributed equally to this work*

Affiliations

1 Wellcome-Wolfson Institute for Experimental Medicine, Queen's University Belfast, Belfast BT9 7BL, UK

Abstract

Temperature is a critical determinant of host–pathogen interactions in the respiratory tract, where influenza A virus (IAV) has adapted to the cooler environment of the upper respiratory tract (URT) to enable efficient replication and transmission. The cold-inducible RNA-binding protein RBM3 is highly expressed in nasopharyngeal tissue and is known to stabilise mRNAs under hypothermic conditions; however, its role during viral infection has not been defined.

Here, we identify RBM3 as a key host factor that facilitates IAV replication at sub-physiological temperatures. siRNA-mediated depletion of RBM3 significantly impaired viral replication, while its constitutive overexpression at 37°C restored replication to levels typically observed at 33°C. Mechanistically, RBM3 binds directly to viral nucleoprotein (NP) mRNA, prolongs its half-life, and promotes the formation of cytoplasmic ribonucleoprotein granules. This effect was abolished in an RNA-binding-deficient RBM3 mutant, confirming the requirement for direct RNA interaction. Crucially, this positive regulation of NP mRNA was validated in well-differentiated primary nasal epithelial cells, highlighting the physiological relevance of RBM3 in the human URT.

These results reveal a temperature-sensitive host–virus interaction that promotes IAV replication in the cooler URT, a key site for viral shedding and transmission. By linking environmental temperature, host RNA-binding proteins, and viral mRNA stability, this study uncovers a novel mechanism of respiratory virus adaptation and identifies RBM3 as a potential therapeutic target for limiting early-stage viral replication and transmission.

Author Summary

To establish productive infection and ensure transmission, respiratory viruses such as influenza A virus (IAV) must adapt to the diverse environments of the human respiratory tract. One key challenge is the temperature gradient that exists between the upper and lower respiratory tract. The upper respiratory tract (URT), the main site of viral entry and transmission, maintains a lower physiological temperature (~33°C) than the lower respiratory tract (~37°C), creating a distinct cellular environment. In this study, we investigated how this cooler URT temperature alters the landscape of RNA-binding proteins (RBPs), which play a central role in regulating gene expression after transcription. Using mass spectrometry-based profiling and molecular virology approaches, we identified a cold-inducible RBP, RBM3, as significantly enriched at 33°C and acting as a key host factor during IAV infection. We show that RBM3 binds directly to viral nucleoprotein (NP) mRNA, promoting its stability and forming cytoplasmic granules that enhance the production of infectious virions. Importantly, disrupting RBM3's RNA-binding ability abolished this proviral effect. These findings reveal that RBM3, elevated in the cooler URT environment, directly supports IAV replication. This work highlights how subtle physiological differences in host tissue can reshape post-transcriptional regulation and influence the outcome of respiratory virus infection.

54 ## Introduction

55 Respiratory viruses remain an ever-present pandemic concern, in part due to their efficient
56 airborne mode of transmission [1]. While severe pathology from respiratory viruses such as
57 influenza A virus (IAV) or SARS-CoV-2 is typically associated with replication in the lower
58 respiratory tract (LRT), transmission predominantly occurs via small droplets and aerosols
59 expelled from the upper respiratory tract (URT) [1–4]. Thus, advancing research into the
60 unique cellular environment of the nasopharyngeal epithelium is critical to deepening our
61 understanding of respiratory virus transmission [5] and will ultimately support public health
62 efforts to develop the next generation of nasal vaccines that boost mucosal immunity [6,7].

63 A key feature of this URT environment is its lower physiological temperature, with
64 nasopharyngeal epithelial cells typically residing at or below 33°C—several degrees cooler
65 than the average core body temperature of 37°C [8]. Though seemingly minor, this
66 temperature difference has far-reaching effects on cellular processes, including viral
67 replication kinetics [9]. Because molecular interactions and reaction rates are governed by
68 thermodynamic principles, temperature is a fundamental variable in regulating biochemical
69 activity. Accordingly, the interaction landscape—including RNA and protein folding, stability,
70 and binding—is substantially altered under cooler conditions [10]. These changes can lead
71 to RNA or protein misfolding [10–12], and, crucially, to temperature-sensitive differences in
72 RNA-binding protein (RBP) affinities for target RNAs, with wide-ranging effects on post-
73 transcriptional regulation [13].

74 Temperature-dependent variation in RBP–RNA binding has significant implications for mRNA
75 spatial localisation, stability, and translation, processes that can influence viral RNA
76 processing and immune evasion [14]. While prior studies have observed temperature-driven

77 changes in transcript and protein abundance [15,16], it remains poorly understood how
78 growth temperature alters the global landscape of RBPs that bind to cellular mRNAs—
79 collectively known as the RBPome.

80 The central aim of this study was to characterise the post-transcriptional environment
81 encountered by respiratory viruses, with a focus on IAV, and to determine how altered
82 growth temperature affects viral mRNA regulation. Specifically, we profiled the mRNA-
83 bound RBPome of lung epithelial cells (A549 cells) grown at 37°C and 33°C, mimicking LRT
84 and URT temperatures, respectively. Recent studies have highlighted the critical role of the
85 host RBPome in shaping viral replication by regulating nuclear export [17], translation [18],
86 and genome replication [19], underscoring the importance of this approach [18,20].

87 Our data reveal extensive temperature-dependent variation in RBPs associated with cellular
88 mRNAs, identifying large sets of RBPs whose binding is either enriched or depleted at 33°C
89 relative to 37°C. Among the most striking findings was the cold-induced enrichment of RNA
90 Binding Motif 3 (RBM3), a well-characterised cold-shock protein known to support cell
91 survival under hypothermic stress [21,22]. Notably, RBM3 was recently identified by our
92 group in an IAV mRNA interactome screen [23]. Here, we build on that work and
93 demonstrate that RBM3, by stabilising viral transcripts, acts as a pro-viral host factor during
94 IAV infection in A549 cells.

95 Crucially, we validate these findings in well-differentiated primary nasal epithelial cells
96 (PNECs) derived from multiple human donors. Using antisense oligonucleotide (ASO)-
97 mediated induction of RBM3 expression [24] followed by infection, we show that elevated
98 RBM3 enhances IAV replication in this physiologically relevant URT model.

99 Together, these findings reveal that RNA regulation in the URT occurs within a distinct post-
100 transcriptional landscape, shaped by cooler tissue temperature. This environment
101 profoundly impacts viral replication dynamics and represents a key barrier that respiratory
102 viruses, such as IAV, have overcome to establish infection and achieve transmission.
103 Understanding these adaptations not only provides new insights into viral evolution and
104 host–pathogen interactions but also offers a foundation for developing temperature-
105 sensitive antiviral strategies and next-generation respiratory vaccines.

106 **Results**

107 The cold RBPome of A549 cells reveals RBM3 as a significantly enriched mRNA interactor

108 As previously mentioned, the temperature gradient normally observed in the respiratory
109 tract is known to yield distinct variations in cellular transcriptomes and proteomes [15,16]
110 (Figure 1A). To identify specific RBPs that are differentially regulated through temperature,
111 we employed RNA Interactome Capture (RIC) [25] on A549 cells incubated for 48 h at 33°C
112 or 37°C. This method allowed for the purification and identification of poly(A) RNA-binding
113 RBPs via UV crosslinking and mass spectrometry (Figure 1B). Quality control of the protein
114 samples to be analysed by MS was assayed by silver staining, highlighting the presence of
115 distinct protein compositions between experimental conditions (Figure 1C). We observed
116 clear differences in band patterns between the 33°C and 37°C in the pulldown samples
117 indicative of the differences between the two proteomes, which were evaluated by LC-
118 MS/MS. The resulting dataset was analysed for enrichment of RBPs in the 33°C compared to
119 the 37°C samples (Figure 1D). Adjusted P values were calculated with a cutoff of $p<0.05$.
120 Between these datasets, we identified a considerable number of RBPs that were
121 preferentially enriched in either temperature. Interestingly, a total of 209 RBPs were shared
122 between 33°C and 37°C (Figure 1E and 1F). Of the total 423 RBPs identified across all
123 datasets, 296 were found to be significantly regulated by alterations in growth temperature.
124 Those that were present in both datasets, but significantly enriched at 33°C, included RBM3,
125 YBOX1, HNRNPC, RBM47 and SND1 (Supplementary Table 1 and 2). Overall, these datasets
126 are important evidence that the RBP environment of the cell is very plastic. Several factors
127 are selectively overrepresented at cold temperatures and thus could play a role in
128 respiratory virus infections.

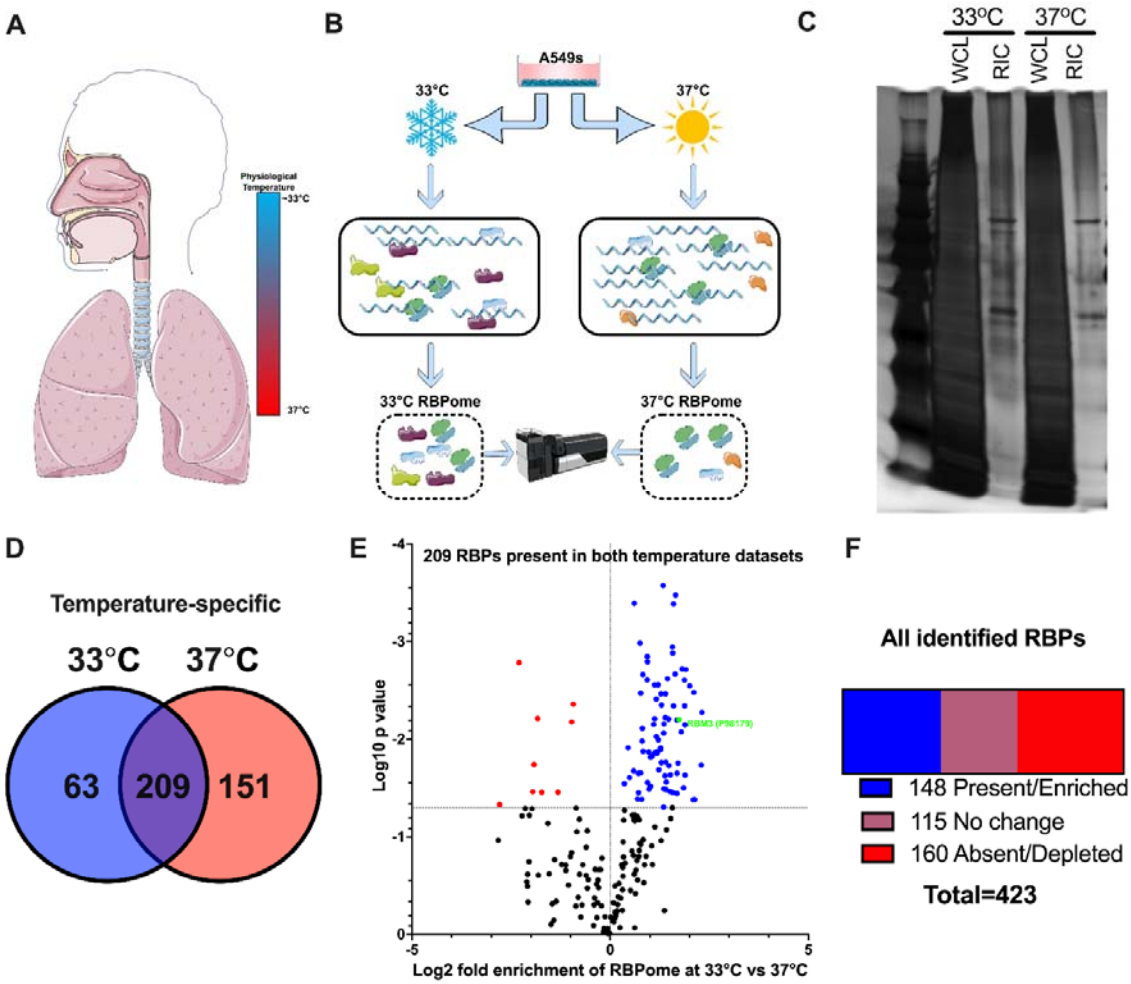

Figure 1 – Cooler growth temperatures vastly alter the RBPome of A549 cells.

(A) *Schematic representation of the temperature gradient between the URT and LRT.* ***(B)*** *Schematic of the workflow for RIC in A549 cells incubated at 33°C or 37°C.* ***(C)*** *Representative silver stain of a gel with the RIC whole cell lysate input (WCL) and pulldown (RIC) samples from protein populations at 33°C and 37°C.* ***(D)*** *Venn diagram showing RBPs present in either 33°C datasets, 37°C datasets or both.* ***(E)*** *Volcano plot showing the enrichment of RBPs isolated from A549 33°C and 37°C pulldown samples.* ***(F)*** *Representation of the proteins significantly altered between datasets, whether by presence/absence or enrichment/depletion. Datasets derived from 3 independent biological samples.*

RBM3 is a positive regulator of IAV replication in A549s, mediated by its RNA-binding activity

One of the top hits enriched in the 33°C dataset was RBM3. This cold-inducible protein was recently identified by us and our colleagues when performing an IAV A/WSN/33 NP mRNA interactome screen [23], and therefore presented an attractive option as an RBP that could play a role in IAV replication in the URT. Firstly, to investigate whether RBM3 impacts IAV replication we performed siRNA-mediated knockdown of RBM3 in A549 cells, followed by infection by WSN at an MOI 0.01 for 48 h. qPCR analysis confirmed effective knockdown

144 with a >95% decrease in RBM3 mRNA levels compared to a nonspecific control siRNA (NSC)
145 (Figure 2A). Total RNA was harvested at 0, 8, 24 and 48 hours post infection (hpi), and levels
146 of viral mRNA were analysed via qPCR. Overall, depletion of RBM3 resulted in a significant
147 decrease in viral HA, NA, NP and M2 mRNA at 24 and 48 hpi (Figure 2B and Supp Figure 1).
148 Most notably, we observed a nearly four-fold decrease in levels of NP mRNA at 24 hpi
149 (Figure 2B). Not surprisingly, this negative impact on viral transcript levels translated
150 through to virus production, resulting in a significant drop in viral titres below the level of
151 detection (Figure 2C).

152 Recent work shows HNRNPH1 controls RBM3 via poison-exon splicing: inclusion of exon 3a
153 in RBM3 pre-mRNA triggers NMD [25], and weak HNRNPH1 binding at 37 °C permits exon
154 inclusion (low RBM3), whereas stronger binding at 30–33 °C excludes exon 3a, boosting
155 RBM3 levels [13]. In A549s transfected with siNSC or siH1 for 48 h and then treated ±CHX for
156 16 h, RT–PCR spanning exons 3–4 revealed exon 3a only in siH1+CHX samples (Supp Fig 2A),
157 and qPCR showed an ~11-fold greater inclusion versus siH1+DMSO (Supp Fig 2B). siH1 also
158 reduced RBM3 mRNA (Supp Fig 2C). After WSN infection (MOI 0.01), siH1 cells had
159 significantly lower NP mRNA at 0–48 hpi (Supp Fig 2D) and reduced viral titres (Supp Fig 2E).
160 Thus, HNRNPH1 modulates RBM3 expression by poison-exon regulation, affecting IAV
161 replication.

162 On identifying RBM3 as a potentially important RBP during IAV replication, we sought to
163 determine whether this pro-viral phenotype arises from a direct interaction between RBM3
164 and viral RNA. However, as evidenced from the RIC MS, the cold environment affects the
165 host globally, and it would be difficult to ascertain the effect of RBM3 alone on viral
166 replication at 33°C. To circumvent this limitation, a cell line expressing cold-induced levels of
167 RBM3 at 37°C was needed. First, a panel of cell lines commonly used to study respiratory

168 viruses was assessed to determine their cold responsiveness, quantified by their ability to
169 induce RBM3 when cultured at 33°C for 48 h. Primary nasal epithelial cells (PNECs) were
170 used as a positive control as it was expected that these would be highly responsive to cooler
171 growth temperatures. RNA was extracted and the levels of RBM3 expression were
172 quantified by qPCR, normalised to the levels observed with culturing at 37°C for each cell
173 type (Figure 2D). While PNECs were the greatest responders, with an approximate 7-fold
174 increase in RBM3 mRNA levels, A549s and 293Ts both demonstrated a >3-fold increase in
175 RBM3 levels. Considering that immortalised cells can be manipulated to a greater extent
176 that PNECs, we proceeded to use A549s to develop greater mechanistic insights into the
177 role of RBM3 during IAV infection. A lentivirus-mediated stably overexpressing RBM3-Flag,
178 clonal A549 cells line, termed A549-RBM3+, was established that could be cultured at 37°C.
179 Upon quantification by qPCR, RBM3 levels were found to be >3-fold increased over an
180 empty vector control line (Figure 2E), mimicking the levels seen upon culturing of parental
181 A549s at 33°C. Viral production was then quantified in these A549-RBM3+ cells, with RBM3
182 overexpression inducing a significant increase in viral titres of >3.5-fold (Figure 2F).

183 RBM3 is composed of two major domains; an RNA Recognition Motif (RRM) found at the C-
184 terminus, and an N-terminus arginine-glycine rich (RGG) domain (Figure 2G) [26]. The
185 former contains two highly conserved RNA binding regions, RNP2 and RNP1. After
186 establishing the binding between NP mRNA and RBM3, we proceeded to investigate how an
187 RNA-binding null mutant RBM3 would affect viral replication. We hypothesised that any
188 pro-viral function would be lost through ablation of RNA-binding. To test this, we created an
189 RBM3 RNA-binding null mutant cell-line, in which mutations were introduced to substitute
190 phenylalanine (F) residues within RNP2 and RNP1 to leucine (L) (Figure 2G). Previous studies
191 have shown that single L>F substitutions within RNP motifs disrupt the RNA binding ability

192 [27]. When viral titres from infected A549-RBM3+ and A549-RBM3 mutant cell lines were

193 compared (Figure 2H), we observed a significant >95% decrease in titres from the RBM3

194 mutant cells.

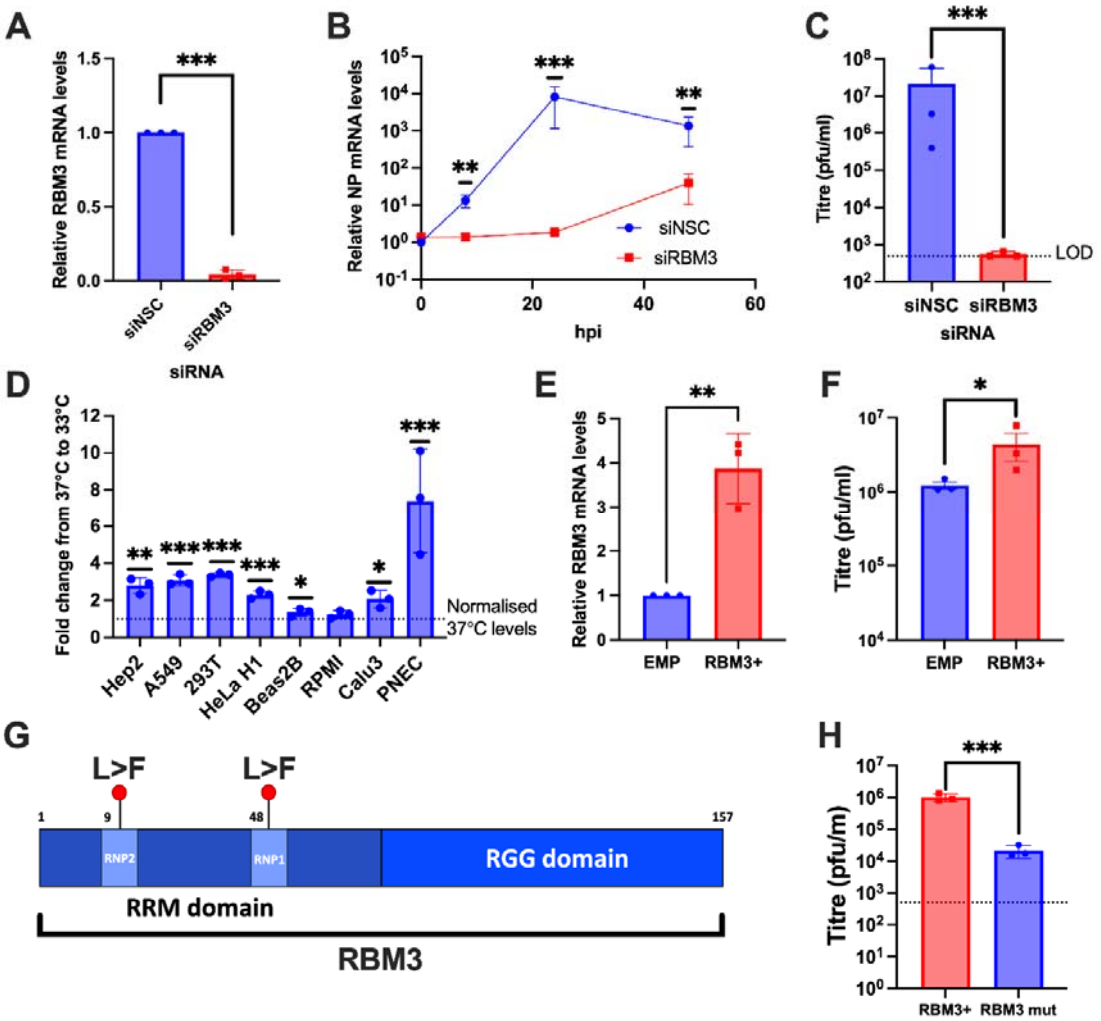

195

196 *Figure 2 – Reducing RBM3 levels in A549 cells greatly inhibits IAV replication.*

197 ***(A)*** *Quantification of RBM3 knockdown using RBM3-targeting siRNAs (siRBM3) compared to a nonspecific control siRNA*
198 *(siNSC).* ***(B)*** *Transcription levels of NP mRNA in siRBM3 or siNSC treated A549 cells infected with WSN at 37°C.* ***(C)*** *Viral titres*
199 *72 hpi with WSN MOI 0.01 in siRBM3 or siNSC treated cells.* ***(D)*** *Cold-responsiveness of a panel of cell lines and primary*
200 *nasal epithelial cells (PNECs) as determined by the induction of RBM3 expression by qPCR over 48 h and normalised to 37°C*
201 *levels.* ***(E)*** *Generation of a lentiviral RBM3 overexpression (RBM3+) A549 cell line alongside a control empty vector line*
202 *(EMP).* ***(F)*** *Titres of WSN at 72 hpi after an MOI 0.01 infection in EMP or RBM3+ A549 cells.* ***(G)*** *Schematic representation of*
203 *RBM3. Single nonsense mutations were introduced into the RNA binding domains, RNP2 and RNP1, creating an RNA-*
204 *binding null mutant RBM3.* ***(H)*** *A549-RBM3+ or A549-RBM3 mut cells were infected at MOI 0.01 with WSN for 48 hours.*
205 *Supernatants were harvested and titrated. Dotted line indicates the limit of detection. Significance was determined using*
206 *Student's t-test with *=p<0.05, **=p<0.01 and ***=p<0.001.*

207

208 With these cell lines in place, a direct interaction between RBM3 and viral transcripts could
209 next be established. To directly visualise the interaction between RBM3 and viral NP mRNA,
210 we employed proximity ligation assay coupled with fluorescence in situ hybridisation (PLA-
211 FISH) [28], a technique adapted here for the first time in the context of virus-infected cells
212 (Figure 3A). This approach revealed prominent cytoplasmic PLA signals in cells expressing
213 wild-type (WT) RBM3, indicating a specific and spatially distinct interaction with NP mRNA
214 (Figure 3B). In contrast, cells expressing either an empty vector or the RNA-binding-deficient
215 RBM3 mutant exhibited only low background signal, consistent with the loss of RNA-binding
216 capability. Notably, in WT RBM3-expressing cells, PLA spots were especially enriched at the
217 cytoplasmic face of the nuclear membrane. This localisation pattern may suggest that RBM3
218 engages NP mRNA soon after nuclear export, potentially stabilising viral transcripts at an
219 early post-transcriptional stage. These findings validate the specificity of RBM3–NP mRNA
220 interactions and highlight the utility of PLA-FISH in mapping host–viral RNA contacts with
221 subcellular resolution.

222 To further validate a direct interaction between RBM3 and NP mRNA we performed CLIP-
223 qPCR in A549-RBM3+ cells infected at MOI 3 for 6 h, then UV crosslinked, and subjected to
224 FLAG immunoprecipitation or an IgG control. The covalently bound RNA was then released
225 by proteinase K digestion, purified and analysed by qPCR. Flag-tagged RBM3 was efficiently
226 pulled down by an anti-Flag immunoprecipitation (Figure 3C & Supp Figure 3), with Actin
227 used as a control to show that this enrichment was specific. RBM3-bound RNA was
228 evaluated by qPCR to determine whether NP mRNA is strongly enriched in RBM3 pulldowns
229 (Figure 3D), due to the presence of multiple predicted high confidence motifs. We also
230 quantified levels of HA mRNA as a likely non-interactor and Actin mRNA, as a host mRNA.
231 We observed a strong and significant enrichment of NP mRNA between the RBM3-Flag and

232 IgG control samples, while no enrichment in HA or Actin levels was observed, indicating little
233 or no binding with RBM3. Taken together, these data collectively establish a direct
234 interaction between RBM3 and NP viral mRNA transcripts, and that this predominantly
235 takes place in the cytoplasm. Finally, using RBPmap [29] and the published RBM3 binding
236 motif (minimally GSNGSNG) [30], we generated a prediction of the number of RBM3 high-
237 confidence binding motifs on WSN transcripts (Figure 3E). While every transcript contained
238 at least 1 putative RBM3 motif with $p<0.05$, NP mRNA was predicted to have multiple highly
239 significant binding motifs with 3 sites of $p<0.001$. Collectively, these data demonstrate that
240 RBM3 directly interacts with NP mRNA upon infection.

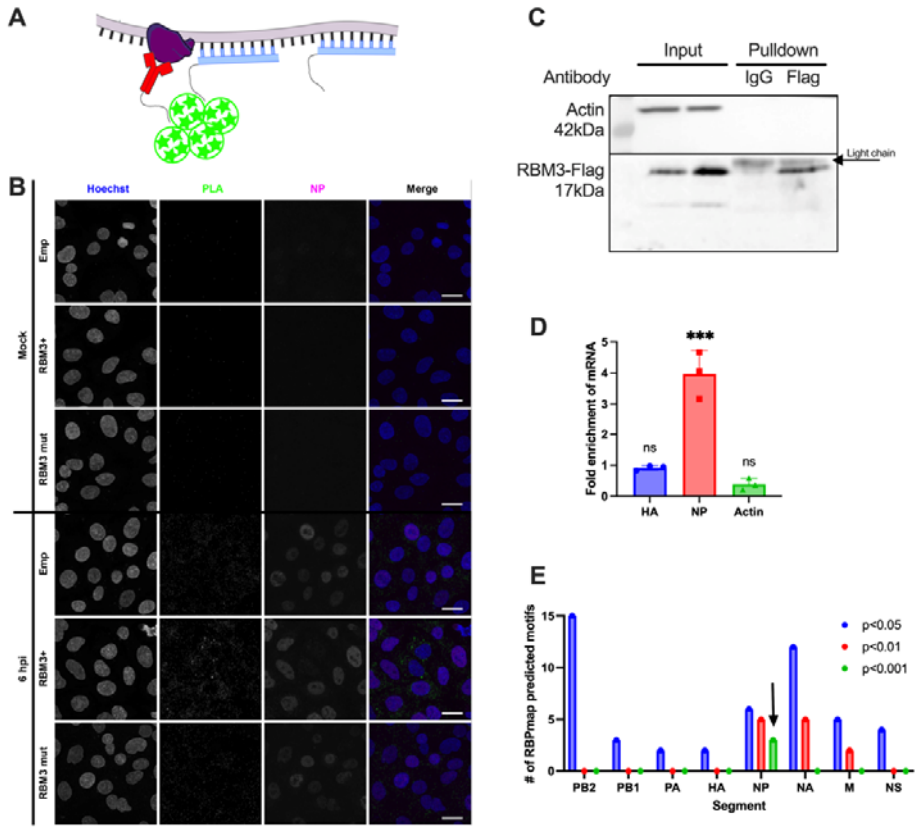

241

242 *Figure 3 – RBM3 directly associates with viral transcripts, increasing overall viral replication.*

243 ***(A)*** *Schematic of PLA-FISH, used to confirm a tight proximity between an RBP and a target mRNA, and the intracellular*
244 *localisation of this interaction.* ***(B)*** *Representative PLA-FISH images showing specific cytoplasmic NP mRNA–RBM3*
245 *interactions in WT RBM3-expressing cells, with prominent signal observed near the nuclear periphery, while only*
246 *background signal is detected in empty vector and RBM3 mutant controls. n=60 cells.* ***(C)*** *Western blot showing input and*

247 *pulldown samples for CLIP-qPCR, blotting for Actin and overexpressed RBM3-Flag.* ***(D)*** *qPCR quantification of the RNA*
248 *extracted from CLIP samples demonstrated a significant increase in viral NP mRNA levels with minimal difference in HA or*
249 *Actin transcript levels, when comparing RBM3 to IgG control pulldowns.* ***(E)*** *RBPmap predicted RBM3 binding motifs for*
250 *each WSN positive strand segment, separated by predicted confidence of each motif.*

251 Overexpression of RBM3 and subsequent binding to NP mRNA stabilises transcripts

252 Having confirmed the interaction between RBM3 and NP mRNA, we next sought to identify
253 how this interaction positively regulates WSN replication. Previous reports have suggested
254 that RBM3 may stabilise certain bound transcripts in neuronal cells [21,22]. Given this
255 context, we next explored the stability of a subset of viral transcripts in the A549-RBM3+ or
256 empty vector A549 cells. Cells were infected with WSN at an MOI 3 for 6 h, then treated
257 with actinomycin D to prevent further cellular and viral transcription [31]. Transcript levels
258 were quantified hourly over 5 timepoints from 0-4 h post-actinomycin D treatment. The
259 data were plotted to visualise the decay of RNA over this treatment period (Figure 4), with a
260 one-phase decay model fitted to the data using a least squares regression. Observed
261 differences in RNA stability were significantly different between cell lines and were assessed
262 by comparing the decay constant (k) values using an extra sum-of-squares F test, with
263 $p<0.05$ deemed significant. Although no significant effect on the stability of viral HA or M2
264 mRNA was observed (Figure 4A & B), a clear and significant increase in stability was
265 quantified for NP mRNA with a >70% increase in RNA half-life (Figure 4C). Actinomycin D
266 assays were then performed in A549-RBM3+ or the RBM3 RNA-binding mutant cell line after
267 IAV infection. These revealed a loss of the stabilisation phenotype in the RBM3 mutant cells
268 for viral NP transcripts as well as GAPDH (Figure 4D and Supp Figure 4). Interestingly, we
269 also observed that overexpression of RBM3 significantly and positively regulated cellular
270 GAPDH levels (Supp Figure 4A), with this phenotype again obviated in the RBM3mut cells.
271 This suggests that RBM3 stabilisation is a direct result of RBM3 binding to target transcripts,
272 and that this is likely a form of cellular post-transcriptional regulation for transcripts such as

273 GAPDH, YAP1 [21] or GAS6 [22]. This mechanism is then seemingly exploited by IAV during
274 infection to promote viral transcript stability upon nuclear export, and overall viral
275 replication.

276 To be certain of our conclusions we employed a minimalist tethering approach. We set up a
277 reporter system in which 293T cells were transfected with a Renilla Luciferase encoding for
278 BoxB hairpins in the 3' UTR, and either WT RBM3 or LambdaN (λN)-RBM3 fusion protein
279 (Figure 4E). The 19 nt BoxB hairpin acts as the target sequence for λN binding and fusion of
280 λN with an RNA-binding protein allows for elucidation of the RBP's function on the BoxB-
281 encoded reporter RNA [32]. Actinomycin D assays were repeated 48 hours post-transfection
282 and levels of luciferase RNA were assessed by qPCR. A significant enhancement in transcript
283 half-life was observed upon expression of the fused λN-RBM3 protein (Figure 4F), providing
284 further evidence that supports the role of RBM3 as an mRNA stabilising agent.

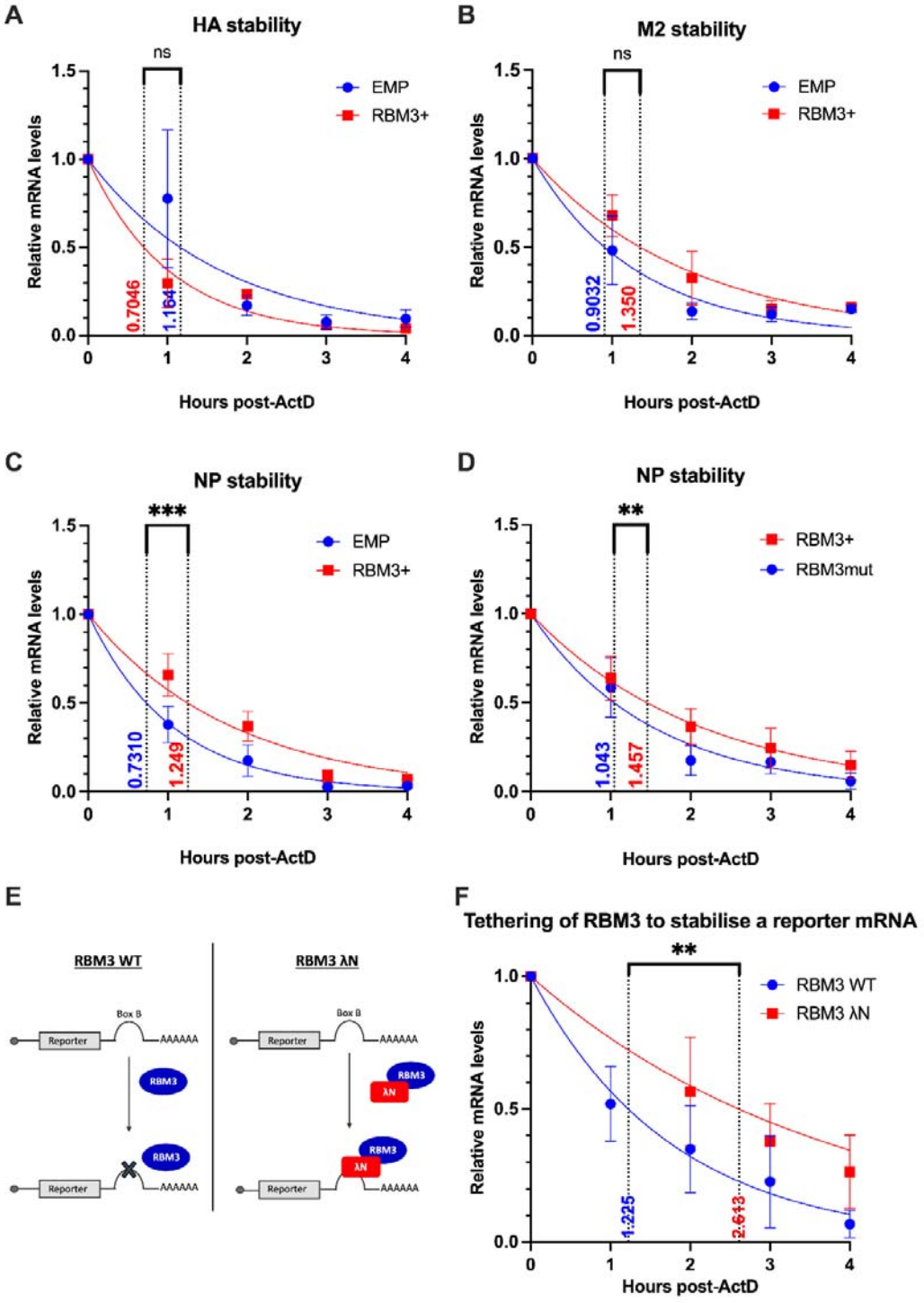

Figure 4 - RBM3 is a stabilising agent through directly binding to target mRNA including IAV NP mRNA.

*Transcript stability in empty vector (EMP) or RBM3 overexpression (RBM3+) A549 cells was established by an actinomycin D (ActD) assay commenced at 6 hpi. Viral transcripts HA **(A)**, M2 **(B)** and NP **(C)** were quantified over 5 hours with transcript half-life quantified by a one-phase decay using a least squares regression. **(D)** The same assay was performed in RBM3+ or the RBM3 RNA-binding mutant (RBM3mut) cell lines, with half-life quantified. **(E)** Schematic representation of the tethering reporter assay. **(F)** 293T cells were transfected with a Luciferase BoxB reporter alongside either WT RBM3 or fused λN-*

292 *RBM3. Cells were treated with Act D 48 hours post-transfection. Luciferase transcripts were quantified over 4 hours with*
293 *transcript half-lives quantified by a one-phase decay using a least squares regression.*

294 RBM3-NP mRNA complexes induce granule formation

295 IF analysis revealed striking cytoplasmic granule formation in WSN-infected cells
296 overexpressing wild-type RBM3 (WT). At both 6 and 8 hpi, RBM3 localised in multiple
297 discrete cytoplasmic foci (white arrows), which strongly colocalised with viral NP mRNA
298 detected by smiFISH, suggesting the assembly of RNA-protein granules involving both RBM3
299 and viral transcripts (Figure 5). These granules were consistently observed across multiple
300 fields but noticeably increased in frequency between 6 and 8 hpi, implying that rising levels
301 of NP mRNA proliferated the formation of these granules (Figure 5).

302 In contrast, cells expressing the RNA-binding-deficient RBM3 mutant (MUT) or empty vector
303 (EMP) did not display granule formation at either time point. In these cells, RBM3 staining
304 was diffuse, and NP mRNA remained evenly distributed in the cytoplasm without foci
305 (Figure 5). This absence of granules in MUT and EMP conditions highlights the requirement
306 for RBM3's RNA-binding capacity and sufficient protein expression for granule formation.
307 The consistent colocalisation of RBM3 and viral mRNA in the WT condition supports a model
308 in which, when expressed to sufficient levels, RBM3 drives the assembly of cytoplasmic RNA
309 granules during infection, potentially stabilising viral transcripts or modulating their
310 localisation.

311

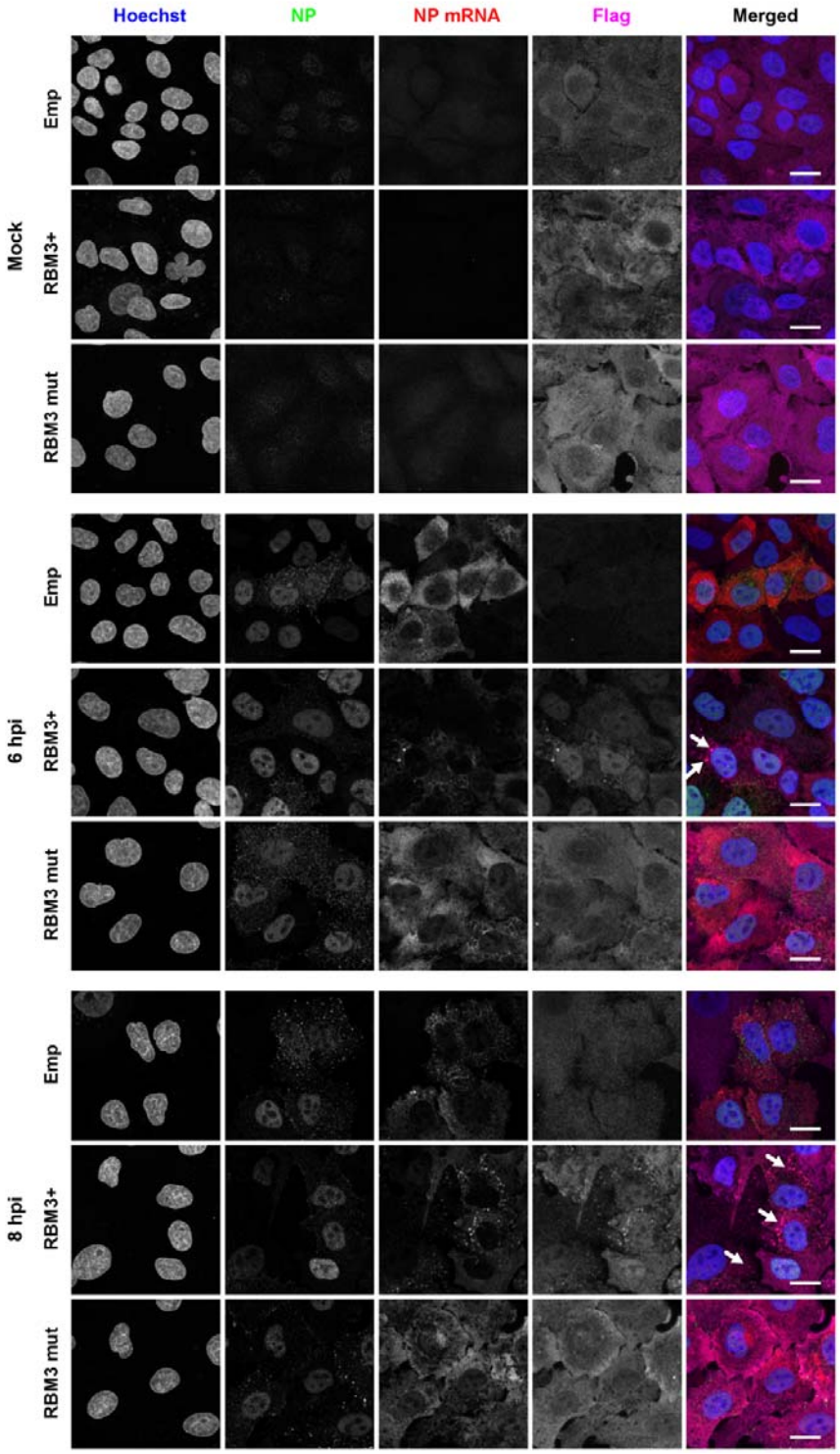

Figure 5 – Formation of RBM3 and NP mRNA granules late in infection.

smiFISH of A/WSN/33 NP mRNA (Red) in Mock and infected A549-Emp, A549-RBM3+ and A549-RBM3 mut cells (MOI5, 6/8 hpi) was performed to determine the subcellular localisation of NP mRNA and to assess the colocalisation with RBM3+/mut. Cells were stained to detect NP (green), Flag (Magenta) and Höchst (Blue). Scale Bar: 10 µM. Z stacks were acquired on Leica STELLARIS ONE 660 tauSTED Nanoscope with a 100x objective with 1.4 NA. Images were analysed using Fiji/ImageJ version 1.54f.

319

320 ASO-mediated increase of RBM3 levels in primary cells promotes overall viral replication

321 Finally, we wanted to determine whether RBM3-mediated increase of overall viral
322 replication would be mirrored in PNECs. Previous studies have determined that targeted
323 ASO treatment of the RBM3 poison exon Ex3a in immortalised cell lines can result in the
324 exclusion of the poison exon, preventing NMD of RBM3 transcripts, and thus increasing
325 overall RBM3 levels, effectively mimicking the function of HNRNPH1 [24]. Treatment of
326 A549 cells with this previously published Ex3a-specific ASO for 48 h resulted in an almost 4-
327 fold increase in RBM3 transcript levels compared to that of a non-targeting control (Figure
328 6A), confirming its effectiveness. Next, ASO treatment was applied apically to PNEC cultures
329 from 3 donors. Primary cells are much less permissive to transfection, therefore, ASO
330 treatment would be predicted to be much less effective at inducing RBM3 in these cultures.
331 Nevertheless, we observed a robust and significant ~50% increase in RBM3 transcript levels
332 after 48 h compared to the control ASO for all 3 donors (Figure 6B). Following this, we
333 subjected PNEC cultures from the same 3 donors to ASO treatment followed by infection
334 with WSN for 48 h. We then evaluated viral replication in these PNECS by quantification of
335 viral RNA levels at 48 hpi. A significant increase in both NP mRNA and vRNA levels was
336 observed by qPCR for each donor upon treatment with the Ex3A-specific ASO, with mRNA
337 levels on average more than doubling after Ex3a ASO treatment (Figure 6C). These data
338 confirm our earlier observations that increasing RBM3 levels positively regulates IAV
339 replication, in a highly relevant human respiratory epithelial model of infection.

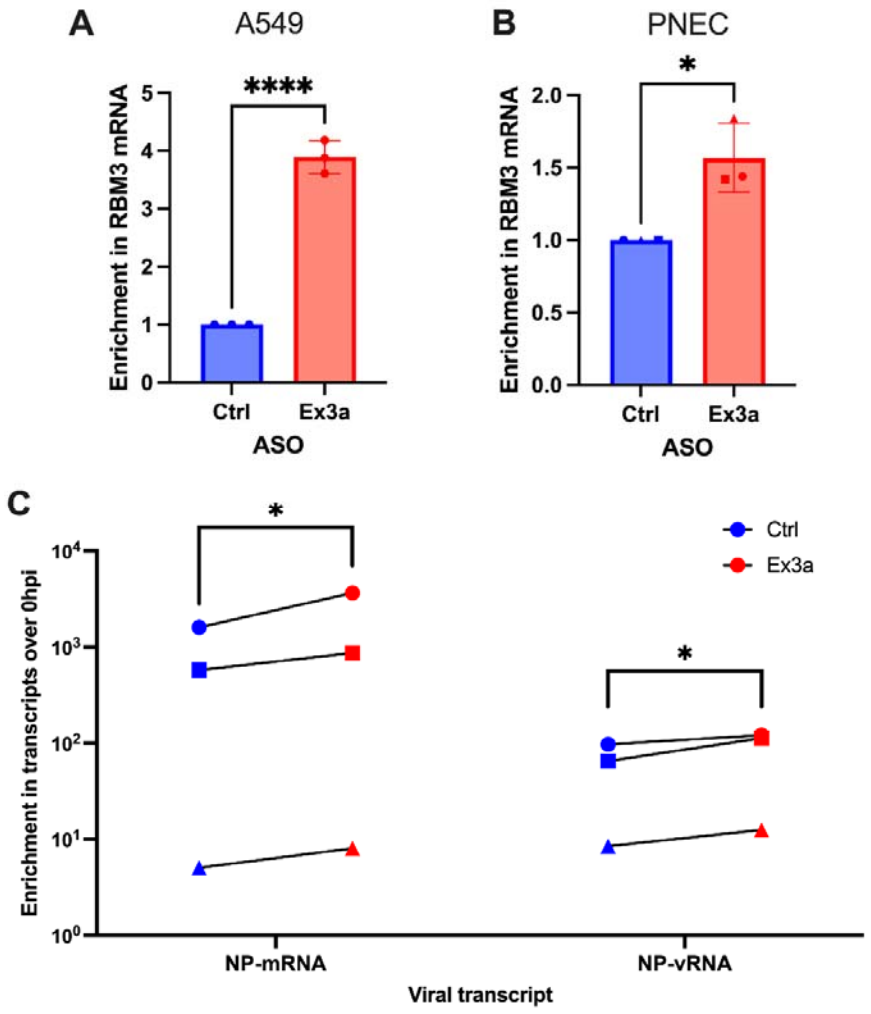

Figure 6 - Increasing expression of RBM3 in PNECs significantly increases IAV replication

(A) *Control (Ctrl) or Exon3a (Ex3a) specific ASOs were initially tested in A549 cells to determine their effectiveness in increasing overall RBM3 mRNA levels, with an approximate 4-fold increase observed at 48 h post-transfection.* ***(B)*** *This was replicated in PNECs at 48 h post-transfection where an approximate 50% ASO-mediated increase in RBM3 levels was quantified.* ***(C)*** *Quantifying viral mRNA and vRNA production in 3 donors (indicated by different shaped data points) previously treated with Ctrl or Ex3a ASOs, demonstrated a significant increase in overall viral replication at 48 hpi.*

348 ## Discussion

349 Given the continuing risk of respiratory virus pandemics, due to coronaviruses such as SARS-
350 CoV-2 or zoonotic influenza strains like H5N1, a detailed understanding of virus-host
351 interactions in relevant tissue environments is critical for future preparedness. The upper
352 respiratory tract (URT) is a primary site of viral replication and transmission, particularly the
353 nasopharyngeal epithelium, which functions at cooler temperatures than core body
354 temperature (~33°C vs. 37°C). This cooler environment likely alters host cell biology and, in
355 turn, viral replication dynamics. To reduce transmission, it is essential to understand how
356 viruses exploit host factors in this unique tissue niche.

357 Here, we present a comprehensive, temperature-resolved RBPome, identifying RNA-binding
358 proteins (RBPs) that are differentially associated with mRNAs in A549 cells cultured at 33°C
359 compared to 37°C (Figure 1). This is the first high-resolution characterisation of the cold-
360 adapted RBPome in a context relevant to URT infection. We identified 63 RBPs unique to
361 33°C and 151 unique to 37°C, with 209 shared across both conditions. Among these, the
362 cold-inducible protein RBM3 was significantly enriched at 33°C, suggesting temperature-
363 dependent regulation of host–RNA interactions.

364 RBM3, known to be regulated by HNRNPH1-mediated splicing [13], has been previously
365 implicated in cell survival under cold stress [33,34], and in stabilising mRNAs such as YAP1
366 and GAS6 [21,22]. However, its role in viral RNA regulation remained largely unexplored.
367 Our study uncovers a previously underappreciated role for RBM3 as a direct stabiliser of IAV
368 mRNA, specifically the NP transcript. This discovery positions RBM3 as a critical modulator
369 of viral gene expression in the URT.

370 We employed multiple, orthogonal assays to robustly validate this interaction. RBM3
371 knockdown significantly reduced viral titres and NP mRNA levels (Figure 2B-C, Supp. Fig. 4),
372 while wild-type RBM3 overexpression enhanced replication. In contrast, an RNA-binding-
373 deficient mutant had no effect (Figure 2E-H), underlining the functional importance of
374 RBM3's RNA-binding capacity.

375 To directly assess RBM3–viral RNA interactions, we combined PLA-FISH (to detect close
376 spatial proximity in situ) and CLIP-qPCR (to confirm direct physical association), supported
377 by in silico binding motif prediction via RBPmap [29]. PLA-FISH revealed strong cytoplasmic
378 co-localisation between RBM3 and NP mRNA at 6 hpi, absent in the RNA-binding mutant
379 (Figure 3B), while CLIP-qPCR confirmed direct enrichment of NP mRNA with RBM3 (Figure
380 3C-E).

381 Next, we explored the functional consequences of RBM3 binding on mRNA stability. RBM3
382 overexpression extended NP mRNA half-life (Figure 4C), an effect abolished in the RNA-
383 binding mutant (Figure 4D). We further validated this stabilising effect in a reporter-based
384 tethering assay, where recruitment of RBM3 to a 3' UTR significantly increased RNA stability
385 (Figure 4F). Together, these data demonstrate a clear and direct role for RBM3 in stabilising
386 viral transcripts, independent of indirect host responses.

387 In virus-infected cells, RBM3 overexpression also induced cytoplasmic granule formation
388 that co-localised with viral mRNAs (Figure 5), a phenotype absent in the mutant or under
389 low RBM3 expression. Given RBM3 is naturally upregulated at 33°C, our overexpression
390 model mimics URT-relevant conditions, suggesting that cooler temperatures promote
391 protective RNA granule formation that shields viral mRNAs from decay. This granule-based
392 mechanism likely contributes to elevated viral mRNA levels during infection.

393 To confirm the translational relevance of our findings, we tested whether increasing RBM3
394 levels in primary human nasal epithelial cells would alter IAV replication. Using ASO-
395 mediated induction of RBM3 [24], we observed donor-specific but consistently increased
396 viral replication, as reflected by elevated NP mRNA and vRNA levels (Figure 6). This
397 demonstrates the functional impact of RBM3 in a clinically relevant URT model.

398 Taken together, our data reveal that RBM3 plays a previously unrecognised, yet pivotal role
399 in stabilising IAV NP mRNA, enhancing replication particularly at cooler URT temperatures.
400 This stabilisation may occur via several mechanisms: protection from endonucleolytic
401 cleavage, inhibition of decay factor binding (e.g., exosome complex [35]), enhanced
402 ribosome loading [36], stabilisation of viral RNA structures [37], or modulation of
403 epitranscriptomic marks [38]. Alternatively, RBM3 may promote mRNA sequestration into
404 membraneless organelles already known to influence vRNA trafficking [39].

405 While IAV appears to have evolved to exploit RBM3 for replication efficiency in the URT, this
406 mechanism could be repurposed therapeutically. Given the success of mRNA vaccines for
407 SARS-CoV-2 [40], and ongoing development of nasal vaccine platforms to induce mucosal
408 immunity [41,42], RBM3's RNA-stabilising properties could be harnessed to enhance mRNA
409 stability and translation in future respiratory therapies. Notably, recent advances have
410 shown inhalable mRNA delivery to the airway epithelium in vivo [6], making this a viable
411 direction for translational research.

412 In conclusion, RBM3 is a temperature-sensitive host factor that directly binds and stabilises
413 influenza A virus mRNAs in the URT. Our multi-assay validation, the creation of a novel
414 temperature-specific RBPome, and the identification of a new functional axis in viral RNA
415 biology collectively underscore the originality and impact of this work. Beyond IAV, our
416 findings suggest that cold-inducible RBPs may represent a broader class of modulators

417 shaping respiratory virus replication in epithelial tissues. These insights expand our
418 understanding of host–pathogen interactions under physiologically relevant conditions and
419 open new avenues for therapeutic intervention and pandemic preparedness.
420

421 **Methods**

422 Cells

423 All immortalised cell lines were cultured in DMEM supplemented with 1% Pen-Strep
424 (Thermo Fisher Scientific; 15140122) and 5% FBS (Thermo Fisher Scientific; 10270106) at
425 37°C/33°C and 5% CO_2. Cell lines used were A549s (ATCC; CCL-185), HEK 293Ts (ATCC; CRL-
426 3216), MDCKs (CCL-34), Hep2s (ATCC; CCL-23), HeLa H1s (ATCC; CRL-1958), Beas2Bs (ATCC;
427 CRL-3588), RPMI 2650s (ATCC; CCL-30) and Calu3s (ATCC; HTB-55).

428 Virus stocks and infections

429 IAV WSN (A/WSN/33) stocks were generated from a reverse genetics system previously
430 described [43]. WSN stocks were grown on MDCK cells in IAV growth media consisting of
431 DMEM, Pen-Strep, 0.2% BSA (Merck; A8412), 25mM HEPES (Merck; H0887) and TPCK-
432 trypsin (Merck; T8802) and titrated on MDCK cells by plaque assay.

433 RIC

434 The protocol employed here to capture the RNA interactome of poly(A)+ RNA (RIC) from
435 A549 cells has been described previously [18,25]. However, we made one minor
436 modification. At the time of seeding, 48 h before crosslinking and harvesting, A549 cells
437 were either incubated under the normal growth temperature of 37°C, to determine the
438 37°C RBPome, or incubated in a 33°C incubator, to determine the 33°C RBPome. Cells were
439 grown for 48 h at these conditions before performing UV crosslinking at 254nm and lysis.
440 The remaining steps were followed exactly as has been described previously [25].

441 Protein visualisation

442 Western blotting was performed as has been previously described [44]. Primary antibodies
443 for influenza PA (Thermo Fisher Scientific; Pa5-32223), RBM3 (Proteintech; 14363-1-AP),
444 ACTB (Proteintech; 66009-1-ig), and Flag (Proteintech; 66008-3-ig) were all used at a 1:5000
445 dilution. Proteins bands on blots were visualised by chemiluminescence. Total protein was
446 imaged by silver staining (Thermo Fisher Scientific; 24612), following the manufacturer's
447 protocol.

448 LC-MS/MS and data analysis

449 Mass spectrometry of RIC samples was performed at the Cambridge Centre for Proteomics.
450 Sample treatment, preparation and trypsin digestion were performed as described
451 previously [45]. Data for each sample were acquired on an Orbitrap Fusion Lumos Tribrid
452 mass spectrometer over a 60 min run. No fractionation was performed due to the likely low
453 complexity of the sample. Raw mass spectrometry data was analysed using MaxQuant
454 software (v2.4.7.0) and utilising the Andromeda search engine [46]. The MS/MS spectra
455 were aligned to the Uniprot Homo sapiens protein database, with known mass
456 spectrometry contaminants and reversed sequences also included. The search was
457 performed with trypsin selected as the specific enzyme and a maximum of 2 missed
458 cleavage events allowed. The MS accuracy was set to 10 ppm, then 0.05 Da for the MS/MS.
459 The maximum peptide charge was set to seven and seven amino acids were required for the
460 minimum peptide length. One unique peptide to the protein group was required to call the
461 presence of a specific protein, while a false-discovery rate (FDR) of 1% was set. Statistical
462 analysis to determine enriched proteins in one set of biological samples over another was
463 performed using the intensities quantified by MaxQuant on Perseus software (v2.0.11) [47].
464 First, any potential contaminants, reverse hits or proteins that were not well identified (fell

465 below 1% FDR) were removed. Then only proteins that were identified in at least 2
466 replicates from a single biological condition were utilised. After filtering, the intensities were
467 log transformed (log_2) and statistical significance was calculated by way of an unpaired two-
468 tailed Student's t-test for each protein group. These values were then log transformed (-
469 log_{10}) and the resulting p values and enrichments were graphed as volcano plots. The cutoff
470 for statistical significance was set to $p < 0.05$.

471 siRNA knockdowns

472 A pair of siRNAs targeting the specified mRNA were used in each knockdown experiment,
473 aside from when a single non-specific control siRNA (siNSC) was used. Sequences of these
474 siRNAs are listed in Supplementary Table 3. A final concentration of 20nM total siRNA was
475 used, and these were transfected using Lipofectamine RNAiMAX (Invitrogen; 13778075)
476 following the manufacturer's instructions. A549 cells were seeded and transfected
477 simultaneously and incubated for 24 h, after which media was changed with fresh growth
478 media. Cells were then incubated for a further 24 h prior to infection.

479 IAV qPCR growth curves

480 A549 cells were infected with A/WSN/33 virus at an MOI 0.01 PFU/cell. At 0, 8, 24 and 48
481 hpi RNA was extracted from cells using TRIzol (Invitrogen; 15596026). RNA was isolated and
482 precipitated following the manufacturer's instructions and 200ng was reverse transcribed
483 into cDNA using the ABI cDNA synthesis kit (Applied Biosystems; 4368814). For all cellular
484 targets RT was performed using an oligo dT, while viral RNA underwent separate RT
485 reactions with primers specific to each mRNA or vRNA [48]. These primers are listed in
486 Supplementary Table 4 alongside the primers used for qPCR amplification. All qPCR
487 experiments were performed using SYBR Select Master Mix (Applied Biosystems; 4472908)

488 following the manufacturer's instructions. All qPCR data were quantified using the ΔΔCT
489 method.

490 Establishment of a RBM3 overexpression cell line using a lentiviral vector

491 A lentiviral expression plasmid was generated encoding for either a full length wild-type
492 RBM3 C-terminally tagged with 2X Flag epitope tags (RBM3+), a full-length RNA-binding
493 mutant (RBM3-Mut), containing two single phenylalanine to leucine substitutions within
494 RNP1 (L48F) and RNP2 (L9F), or an empty vector (A549-EMP). A549-RBM3, A549-EMP and
495 A549-Mut were followed by a P2A self-cleaving peptide and a puromycin resistance gene,
496 similar to a system we have published previously [38]. Again, similar to previous
497 publications, we rescued lentiviral particles by co-transfecting 293T cells with the RBM3,
498 RBM3 Mut or EMP lentiviral vector alongside d8.74 (Addgene; 22036) and MD2G (Addgene;
499 12259). At 72 h post-transfection the supernatant was harvested, passed through a 0.45 μm
500 filter and then overlaid onto fresh A549 cells. At 72 h post transduction cells were treated
501 with 2 μg/ml puromycin and left to select for 72 h. Cells were then single cell cloned in 96
502 well plates in the presence of 2 μg/ml puromycin and left to grow for 3 weeks. Single cell
503 colonies were then selected, expanded, and checked by Western blot to confirm the
504 expression of the transgene.

505 PLA-FISH

506 A549 cells expressing Flag, RBM3 WT or RBM3 Mt were seeded on to a 12 mm coverslip in
507 24 well plates. 24 hrs later cells were infected in a synchronised manner with IAV/WSN at an
508 MOI of 5 for 1 hr at 4°C. The infection was allowed to follow through for 6 hrs to allow for
509 peak viral mRNA production. 6 hrs later, cells were fixed with 4% PFA for 15 min at RT, then
510 washed thrice with PBS. Cells were permeabilised with 0.5% Triton X for 10 min at RT, then

511 washed thrice with PBS. Following a protocol adapted from Alagia et al. [28], coverslips
512 were incubated with 30 µl of PLA-blocking buffer in a pre-warmed humidified chamber and
513 incubated for 1 h at 37°C. Cells were incubated with 30 µl of FISH-PLA probe buffer in the
514 humidified chamber in a hybridisation oven at 95°C for 3 min, followed by 18 h incubation at
515 37°C. The next day, coverslips were placed into a 24 well plate and three washes were
516 performed with 2× SSC wash buffer, followed by two washes with PBS at 20°C for 5 min with
517 gentle rocking. Cells were incubated with 30 µl of Duolink Blocking Solution and incubated
518 at 37°C for 1 h. Cells were incubated with 30 µl of primary antibody against Flag (Sigma,
519 F1804) diluted in Duolink Antibody Diluent for 18 h at 37°C in a humidified chamber. The
520 next day, coverslips were placed into a 24 well plate and three washes were performed with
521 pre-warmed Wash Buffer A at 20°C for 5 min with gentle rocking. Cells were incubated with
522 30 µl of Minus PLA probe diluted 1:5 and Phalloidin diluted 1:200 in Duolink Antibody
523 Diluent in a humidity chamber at 37°C for 1 h followed by three washes with Wash Buffer A.
524 Duolink ligase buffer was diluted 1:5 in ddH2O. For 60 µL of ligase reaction solution, 1.5 µL
525 of ligase enzyme was added to 58.5 µL of the diluted Duolink ligase buffer dilution. Cells
526 were incubated with 20 µl of ligase buffer in a humidity chamber at 37°C for 30 min
527 followed by three washes with Wash Buffer A. Duolink amplification buffer was diluted 1:5
528 in ddH2O and protected from light. For a 60 µL of amplification reaction, 0.75 µL of
529 polymerase enzyme was added to 59.25 µL of the diluted Duolink amplification buffer
530 dilution. Cells were incubated with 20 µl of amplification buffer in a humidity chamber at
531 37°C for 1h and 40 min followed by two washes with pre-warmed Wash Buffer B containing
532 1:4000 Hoechst (Abcam; ab228551) in a 24 well plate. Wash steps were performed at 20°C
533 for 10 min with gentle rocking followed by a last wash with 0.01× Wash Buffer B. Coverslips
534 were mounted on to slides with Diamond antifade Mounting medium and imaged the

535 following day on the Leica STELLARIS ONE 660 tauSTED Nanoscope with a 100x objective
536 with 1.4 NA. Z stacks were acquired and analysed using Fiji/ImageJ version 1.54f.

537 CLIP-qPCR

538 The CLIP-qPCR protocol employed here has been published previously [49]. Briefly, A549-
539 RBM3+ cells were seeded one day prior to infection. Cells were infected with A/WSN/33 at
540 an MOI 3 PFU/cell and incubated for 6 h. At 6 hpi media was removed from the cells, before
541 being washed in ice cold PBS. UV crosslinking was performed at 254nm. Cells were then
542 scraped, pelleted and lysed in 250 µl of NP40 lysis buffer (HEPES-KOH pH 7.5 50mM, KCl
543 150mM, EDTA pH 8.0 2mM, NaF 1mM and NP40 0.5%) on ice for 30 min. Lysates were
544 clarified by centrifugation and 10% of the sample was saved as an input and boiled in
545 Laemmli buffer containing 2% β-mercaptoethanol at 95°C for 10 min for western blotting.
546 The remaining 90% of lysate underwent immunoprecipitation with anti-Flag antibody
547 (Merck, F1804) or IgG control antibody coupled to Protein G Dynabeads (ThermoFisher,
548 10004D) for 1 h at room temperature. Beads were then captured, washed five times with 1
549 mL NP40 lysis buffer and three times with PBS. A fraction (10%) of the beads was removed,
550 resuspended in Laemmli buffer and boiled at 95°C for 10 min for Western blotting. The
551 remaining 90% of beads underwent proteinase K digestion (ThermoFisher, EO0491) at 55°C
552 for 60 min to release bound RNA, following the manufacturer's instructions. RNA was then
553 isolated from the digestion by TRIzol LS (ThermoFisher, 10296028) and ethanol precipitation
554 and cDNA were synthesized using oligo dT or A/WSN/33 specific primers [48]
555 (Supplementary Table 4). Quantification of the cDNAs was performed by qPCR, as described
556 below. Fold enrichment of RNA levels was quantified using the ΔΔCT method and
557 normalised to input levels.

558 Actinomycin D assays

559 A549-RBM3+, A549-Mut and A549-EMP cells were seeded at a density of 1 x 10^5 cells/well
560 one day prior to infection. Cells were infected with WSN at a MOI of 3 PFU/cell. At 6 hpi,
561 RNA was harvested from a single well for each cell type, constituting the 0 h timepoint. All
562 remaining infected wells underwent media exchange for growth media containing 2 µg/mL
563 Actinomycin D (SBR00013). RNA was harvested hourly from 7-10 hpi representing 1-4 h post
564 Actinomycin D treatment. RNA underwent cDNA conversion using oligo dT or A/WSN/33
565 specific primers, with the ABI cDNA synthesis kit (Applied Biosystems; 4368814).
566 Quantification of the cDNAs was performed by qPCR, described above. Fold enrichment of
567 RNA levels was quantified using the ΔΔCT method and normalised to either A549-EMP or
568 A549-RBM3 levels.

569 λN tethering assay

570 λN was cloned into a lentiviral expression vector expressing full-length WT RBM3. 293T cells
571 were seeded at a density of 1 x 10^5 cells/mL in a 12-well plate the day before transfection.
572 The following day, cells were transfected with 500 ng of pCI-RLuc-BoxB [50] and 100 ng of
573 either the WT RBM3 or the λN-RBM3 WT expressing plasmids. At 48 hours post-
574 transfection, RNA was harvested from a single well for each transfection to represent a 0h
575 timepoint. All remaining cells were treated with 2 µg/mL Actinomycin D (SBR00013). RNA
576 was harvested by TRIzol hourly up to 4 hours post-treatment. RNA underwent DNaseI
577 (Invitrogen, EN0521) digestion to remove any residual plasmid DNA before cDNA conversion
578 using oligo dT primers with the ABI cDNA synthesis kit (Applied Biosystems; 4368814).
579 Quantification of the cDNAs was performed by qPCR, described above. Fold enrichment of

580 luciferase RNA levels was quantified using the ΔΔCT method and normalised to the
581 corresponding 0 h mRNA levels.

582 Immunofluorescence

583 A549-Emp, A549-RBM3+, A549-RBM3 mut cells were seeded in 24-well plates onto 12 mm
584 coverslips. 24h post seeding, cells were infected with influenza A/WSN/33 at MOI 5. Cells
585 were fixed at 6 hpi with 4% PFA and permeabilised with 70% ethanol for 2 hours at 4°C. Cells
586 were briefly washed with FISH wash buffer (10% SSC, 10% formamide, 80% ddH2O) and
587 incubated O/N at 37°C with smiFISH probes (Supplementary Table 6) against WSN NP mRNA
588 annealed to a Cy3 imager strand, as we have previously described [17]. Cells were washed
589 twice with FISH wash buffer at 37°C for 30 minutes. Cells were stained with primary
590 antibodies Rabbit anti-NP (PA5-32242, Invitrogen) and Mouse anti-Flag (66008-3-ig,
591 Proteintech) to detect RBM3+/mut for 1 hr at 37°C, followed by Goat anti-Ms AF647
592 (A32728, Invitrogen) and Goat anti-Rb AF488 (A11008, Invitrogen) secondary antibodies.
593 Cells were counterstained with Hoechst (ab228551, abcam) and mounted using ProLong™
594 Diamond antifade mounting media (P36961, Invitrogen). Coverslips were imaged with a
595 Leica STELLARIS ONE 660 tauSTED Nanoscope with a 100x objective with 1.4 NA. Z stacks
596 were acquired and analysed using Fiji/ImageJ version 1.54f.

597 Well-Differentiated Primary Airway Epithelial Cell Culture

598 Primary nasal epithelial cells were obtained from Promocell and well differentiated primary
599 nasal epithelial cell (WD-PNEC) cultures were established as described previously [51].
600 Briefly, WD-PNECs were seeded onto collagen coated 6 mm Transwells (Sarstedt,
601 83.3932.041) at $3x10^4$ cells/transwell. Cells were submerged in modified Promocell Airway
602 Epithelial Cell Growth Medium which was replaced on the apical and basal side every 2 days

603 until the cells reached confluency. Once confluent, an air liquid interface (ALI) was initiated
604 by completely removing the apical medium. Cells were differentiated using Pneumacult ALI
605 medium (Stemcell Technologies, #05001) supplemented with hydrocortisone and heparin.
606 For downstream experiments, WD-PNECs were only used when there was extensive cilia
607 coverage and mucus production, clear hallmarks of full differentiation.

608 ASO transfection and IAV infection of cells

609 A549s were transfected with control or Exon 3a targeting ASOs [24] (Supplementary Table
610 5) to initially test whether induction of RBM3 could be achieved in airway cells. ASOs were
611 resuspended in DMEM at a concentration of 1 µM and transfected using Lipofectamine
612 2000 (Invitrogen, 1 µL/mL). At 48 h post-transfection RNA was harvested, cDNA synthesised
613 as described above, and RBM3 levels quantified by qPCR. For WD-PNEC cells, the
614 transfection conditions were the same, with the ASO-containing transfection mix added
615 apically to WD-PNECs. Cells were incubated for 48 h prior to infection with WSN MOI 0.01
616 PFU/cell in DMEM. At 1 hpi, the inoculum was removed and transwells were washed 5 times
617 in DMEM to remove unbound virus. RNA was harvested from WD-PNECS using Trizol™
618 either before infection or at 72 hours post-infection.

619 Statistical analysis

620 Unless otherwise stated, all experiments were performed as 3 independent biological
621 replicates. When bar graphs are used to represent the data, each individual replicate can be
622 observed as a point overlaid on the bar, with error bars indicating standard deviation.
623 Significance was calculated by performing Student's t-test with * indicating $p<0.05$, **
624 indicating $p<0.01$ and *** indicating $p<0.001$.

Acknowledgements

This research was funded in part by an ERC-STG grant, PTFLU 949506 awarded to D.G.C. This research received infrastructure support from the Wellcome-Wolfson Institute for Experimental Medicine at Queen's University Belfast. Authors would like to thank Dr Seyed Mehdi Jafarnejad for providing the plasmids for the BoxB reporter system.

In Figure 1 cells_bilayer icon by Marcel Tisch is licensed under CC0, upper-respiratory-tract icon by Servier https://smart.servier.com/ is licensed under CC-BY 3.0 Unported, lung icon by Servier https://smart.servier.com/ is licensed under CC-BY 3.0 Unported, all protein icons by Servier https://smart.servier.com/ is licensed under CC-BY 3.0 Unported, Liquid_Chromatograph_Mass_Spectrometer icon by DBCLS https://togotv.dbcls.jp/en/pics.html is licensed under CC-BY 4.0 Unported and rna icon by Servier https://smart.servier.com/ is licensed under CC-BY 3.0 Unported. In Figure 3 RNA, oligo, RBP and antibody icons were acquired from the NIAID NIH BIOART under a CC-BY license.

641 **References**

642 1. Lakdawala SS, Jayaraman A, Halpin RA, Lamirande EW, Shih AR, Stockwell TB,
643 et al. The soft palate is an important site of adaptation for transmissible
644 influenza viruses. Nature. 2015;526: 122–125. doi:10.1038/nature15379

645 2. Xie C, Su W, Sia SF, Choy KT, Morrell S, Zhou J, et al. A(H1N1)pdm09 Influenza
646 Viruses Replicating in Ferret Upper or Lower Respiratory Tract Differed in
647 Onward Transmission Potential by Air. J Infect Dis. 2022;225: 65–74.
648 doi:10.1093/INFDIS/JIAB286

649 3. Richard M, van den Brand JMA, Bestebroer TM, Lexmond P, de Meulder D,
650 Fouchier RAM, et al. Influenza A viruses are transmitted via the air from the
651 nasal respiratory epithelium of ferrets. Nature Communications 2020 11:1.
652 2020;11: 1–11. doi:10.1038/s41467-020-14626-0

653 4. Varble A, Albrecht RA, Backes S, Crumiller M, Bouvier NM, Sachs D, et al.
654 Influenza A Virus Transmission Bottlenecks Are Defined by Infection Route and
655 Recipient Host. Cell Host Microbe. 2014;16: 691–700.
656 doi:10.1016/J.CHOM.2014.09.020

657 5. Bisht K, te Velthuis AJW. Decoding the Role of Temperature in RNA Virus
658 Infections. mBio. 2022;13. doi:10.1128/MBIO.02021-22/ASSET/C4C1EBDE-
659 A0D5-410C-9B3C-4C65FBA3C93F/ASSETS/IMAGES/MEDIUM/MBIO.02021-22-
660 F002.GIF

661 6. Suberi A, Grun MK, Mao T, Israelow B, Reschke M, Grundler J, et al. Polymer
662 nanoparticles deliver mRNA to the lung for mucosal vaccination. Sci Transl
663 Med. 2023;15.

664 doi:10.1126/SCITRANSLMED.ABQ0603/SUPPL_FILE/SCITRANSLMED.ABQ0603_
665 MDAR_REPRODUCIBILITY_CHECKLIST.PDF
666 7. McMahan K, Wegmann F, Aid M, Sciacca M, Liu J, Hachmann NP, et al. Mucosal
667 boosting enhances vaccine protection against SARS-CoV-2 in macaques. Nature
668 2023 626:7998. 2023;626: 385–391. doi:10.1038/s41586-023-06951-3
669 8. Eccles R. Why is temperature sensitivity important for the success of common
670 respiratory viruses? Rev Med Virol. 2021;31: 1–8. doi:10.1002/RMV.2153
671 9. Otter CJ, Fausto A, Tan LH, Khosla AS, Cohen NA, Weiss SR. Infection of primary
672 nasal epithelial cells differentiates among lethal and seasonal human
673 coronaviruses. Proc Natl Acad Sci U S A. 2023;120: e2218083120.
674 doi:10.1073/PNAS.2218083120/SUPPL_FILE/PNAS.2218083120.SAPP.PDF
675 10. Pullara P, Alshareedah I, Banerjee PR. Temperature-dependent reentrant
676 phase transition of RNA-polycation mixtures. Soft Matter. 2022;18: 1342–1349.
677 doi:10.1039/D1SM01557E
678 11. Riback JA, Katanski CD, Kear-Scott JL, Pilipenko E V., Rojek AE, Sosnick TR, et al.
679 Stress-Triggered Phase Separation Is an Adaptive, Evolutionarily Tuned
680 Response. Cell. 2017;168: 1028-1040.e19. doi:10.1016/J.CELL.2017.02.027
681 12. Tauber D, Tauber G, Parker R. Mechanisms and Regulation of RNA
682 Condensation in RNP Granule Formation. Trends Biochem Sci. 2020;45: 764–
683 778. doi:10.1016/J.TIBS.2020.05.002
684 13. Lin JQ, Khuperkar D, Pavlou S, Makarchuk S, Patikas N, Lee FC, et al. HNRNPH1
685 regulates the neuroprotective cold-shock protein RBM3 expression through

686 poison exon exclusion. EMBO J. 2023;42: e113168.
687 doi:10.15252/EMBJ.2022113168

688 14. Bonazza S, Courtney DG. Influenza A virus RNA localisation and the interceding
689 trafficking pathways of the host cell. PLoS Pathog. 2025;21: e1013090.
690 doi:10.1371/JOURNAL.PPAT.1013090

691 15. Cugusi S, Mitter R, Kelly GP, Walker J, Han Z, Pisano P, et al. Heat shock induces
692 premature transcript termination and reconfigures the human transcriptome.
693 Mol Cell. 2022;82: 1573-1588.e10.
694 doi:10.1016/J.MOLCEL.2022.01.007/ATTACHMENT/F4235ADB-517D-41B2-
695 B14B-196321576620/MMC5

696 16. Gagnon D, Barry H, Barhdadi A, Oussaid E, Mongrain I, Lemieux Perreault LP, et
697 al. A dataset of proteomic changes during human heat stress and heat
698 acclimation. Scientific Data 2023 10:1. 2023;10: 1–6. doi:10.1038/s41597-023-
699 02809-5

700 17. Bonazza S, Coutts HL, Sukumar S, Turkington HL, Courtney DG. Identifying
701 cellular RNA-binding proteins during infection uncovers a role for MKRN2 in
702 influenza mRNA trafficking. Schwemmle M, editor. PLoS Pathog. 2024;20:
703 e1012231. doi:10.1371/journal.ppat.1012231

704 18. Garcia-Moreno M, Noerenberg M, Ni S, Järvelin AI, González-Almela E, Lenz CE,
705 et al. System-wide Profiling of RNA-Binding Proteins Uncovers Key Regulators
706 of Virus Infection. Mol Cell. 2019;74: 196-211.e11.
707 doi:10.1016/j.molcel.2019.01.017

708 19. Schmidt N, Ganskih S, Wei Y, Gabel A, Zielinski S, Keshishian H, et al. SND1
709 binds SARS-CoV-2 negative-sense RNA and promotes viral RNA synthesis
710 through NSP9. Cell. 2023;186: 4834-4850.e23. doi:10.1016/J.CELL.2023.09.002

711 20. Kamel W, Noerenberg M, Cerikan B, Chen H, Järvelin AI, Kammoun M, et al.
712 Global analysis of protein-RNA interactions in SARS-CoV-2 infected cells reveals
713 key regulators of infection. Mol Cell. 2021 [cited 25 May 2021].
714 doi:10.1016/j.molcel.2021.05.023

715 21. Xia W, Su L, Jiao J. Cold-induced protein RBM3 orchestrates neurogenesis via
716 modulating Yap mRNA stability in cold stress. J Cell Biol. 2018;217: 3464–3479.
717 doi:10.1083/JCB.201801143

718 22. Lin P, Lin C, Diao L. RBM3 Ameliorates Acute Brain Injury-induced Inflammation
719 and Oxidative Stress by Stabilizing GAS6 mRNA Through Nrf2 Signaling
720 Pathway. Neuroscience. 2024;547: 74–87.
721 doi:10.1016/J.NEUROSCIENCE.2024.03.028

722 23. Dupont M, Krischuns T, Gianetto QG, Paisant S, Bonazza S, Brault J-B, et al. The
723 RBPome of influenza A virus NP-mRNA reveals a role for TDP-43 in viral
724 replication. Nucleic Acids Res. 2024;52. doi:10.1093/NAR/GKAE291

725 24. Preußner M, Smith HL, Hughes D, Zhang M, Emmerichs A, Scalzitti S, et al. ASO
726 targeting RBM3 temperature-controlled poison exon splicing prevents
727 neurodegeneration in vivo . EMBO Mol Med. 2023;15. Available:
728 https://www.embopress.org/doi/10.15252/emmm.202217157

729 25. Castello A, Fischer B, Eichelbaum K, Horos R, Beckmann BM, Strein C, et al.
730 Insights into RNA Biology from an Atlas of Mammalian mRNA-Binding Proteins.
731 Cell. 2012;149: 1393–1406. doi:10.1016/j.cell.2012.04.031

732 26. RB Z, XL L, CY Z, DC Y. RNA binding motif protein 3: a potential biomarker in
733 cancer and therapeutic target in neuroprotection. Oncotarget. 2017;8.
734 doi:10.18632/ONCOTARGET.14755

735 27. Serin G, Joseph G, Ghisolfi L, Bauzan M, Erard M, Amalric F, et al. Two RNA-
736 binding domains determine the RNA-binding specificity of nucleolin. J Biol
737 Chem. 1997;272: 13109–13116. doi:10.1074/JBC.272.20.13109

738 28. Alagia A, Ketley RF, Gullerova M. Detecting RNA-protein proximity at DNA
739 double-strand breaks using combined fluorescence in situ hybridization with
740 proximity ligation assay. STAR Protoc. 2023;4.
741 doi:10.1016/J.XPRO.2023.102096

742 29. Paz I, Kosti I, Ares M, Cline M, Mandel-Gutfreund Y. RBPmap: a web server for
743 mapping binding sites of RNA-binding proteins. Nucleic Acids Res. 2014;42.
744 doi:10.1093/NAR/GKU406

745 30. Liu Y, Hu W, Murakawa Y, Yin J, Wang G, Landthaler M, et al. Cold-induced
746 RNA-binding proteins regulate circadian gene expression by controlling
747 alternative polyadenylation. Scientific Reports 2013 3:1. 2013;3: 1–11.
748 doi:10.1038/srep02054

749 31. Ratnadiwakara M, Änkö M-L. mRNA Stability Assay Using transcription
750 inhibition by Actinomycin D in Mouse Pluripotent Stem Cells. Bio Protoc.
751 2018;8. doi:10.21769/BIOPROTOC.3072

752 32. Baron-Benhamou J, Gehring NH, Kulozik AE, Hentze MW. Using the λN peptide
753 to tether proteins to RNAs. mRNA Processing and Metabolism Methods in
754 Molecular Biology . Humana Press; 2004.
755 33. Peretti D, Bastide A, Radford H, Verity N, Molloy C, Martin MG, et al. RBM3
756 mediates structural plasticity and protective effects of cooling in
757 neurodegeneration. Nature. 2015;518: 236–239. doi:10.1038/NATURE14142
758 34. Wellmann S, Truss M, Bruder E, Tornillo L, Zelmer A, Seeger K, et al. The RNA-
759 Binding Protein RBM3 Is Required for Cell Proliferation and Protects Against
760 Serum Deprivation-Induced Cell Death. Pediatric Research 2010 67:1. 2010;67:
761 35–41. doi:10.1203/pdr.0b013e3181c13326
762 35. Schmid M, Jensen TH. The exosome: a multipurpose RNA-decay machine.
763 Trends Biochem Sci. 2008;33: 501–510. doi:10.1016/j.tibs.2008.07.003
764 36. Dresios J, Aschrafi A, Owens GC, Vanderklish PW, Edelman GM, Mauro VP. Cold
765 stress-induced protein Rbm3 binds 60S ribosomal subunits, alter microRNA
766 levels, and enhances global protein synthesis. Proc Natl Acad Sci U S A.
767 2005;102: 1865–1870.
768 doi:10.1073/PNAS.0409764102/SUPPL_FILE/09764FIG7.JPG
769 37. Yang R, Pan M, Guo J, Huang Y, Zhang QC, Deng T, et al. Mapping of the
770 influenza A virus genome RNA structure and interactions reveals essential
771 elements of viral replication. Cell Rep. 2024;43.
772 doi:10.1016/J.CELREP.2024.113833
773 38. Courtney DG, Kennedy EM, Dumm RE, Bogerd HP, Tsai K, Heaton NS, et al.
774 Epitranscriptomic Enhancement of Influenza A Virus Gene Expression and

775 Replication. Cell Host Microbe. 2017;22: 377–386.
776 doi:10.1016/j.chom.2017.08.004

777 39. Alenquer M, Vale-Costa S, Etibor TA, Ferreira F, Sousa AL, Amorim MJ.
778 Influenza A virus ribonucleoproteins form liquid organelles at endoplasmic
779 reticulum exit sites. Nat Commun. 2019;10. doi:10.1038/S41467-019-09549-4

780 40. Morens DM, Taubenberger JK, Fauci AS. Rethinking next-generation vaccines
781 for coronaviruses, influenzaviruses, and other respiratory viruses. Cell Host
782 Microbe. 2023;31: 146–157. doi:10.1016/J.CHOM.2022.11.016

783 41. Sheikh-Mohamed S, Isho B, Chao GYC, Zuo M, Cohen C, Lustig Y, et al. Systemic
784 and mucosal IgA responses are variably induced in response to SARS-CoV-2
785 mRNA vaccination and are associated with protection against subsequent
786 infection. Mucosal Immunol. 2022;15: 799. doi:10.1038/S41385-022-00511-0

787 42. Liew F, Talwar S, Cross A, Willett BJ, Scott S, Logan N, et al. SARS-CoV-2-specific
788 nasal IgA wanes 9 months after hospitalisation with COVID-19 and is not
789 induced by subsequent vaccination. EBioMedicine. 2023;87: 104402.
790 doi:10.1016/J.EBIOM.2022.104402

791 43. Fodor E, Devenish L, Engelhardt OG, Palese P, Brownlee GG, García-Sastre A.
792 Rescue of Influenza A Virus from Recombinant DNA. J Virol. 1999;73: 9679.
793 doi:10.1128/JVI.73.11.9679-9682.1999

794 44. Courtney DG, Chalem A, Bogerd HP, Law BA, Kennedy EM, Holley CL, et al.
795 Extensive epitranscriptomic methylation of A and C residues on murine
796 leukemia virus transcripts enhances viral gene expression. mBio. 2019;10:
797 e01209-19. doi:http://dx.doi.org/10.1101/591545

798 45. Queiroz RML, Smith T, Villanueva E, Marti-Solano M, Monti M, Pizzinga M, et
799 al. Comprehensive identification of RNA–protein interactions in any organism
800 using orthogonal organic phase separation (OOPS). Nature Biotechnology 2019
801 37:2. 2019;37: 169–178. doi:10.1038/s41587-018-0001-2
802 46. Cox J, Mann M. MaxQuant enables high peptide identification rates,
803 individualized p.p.b.-range mass accuracies and proteome-wide protein
804 quantification. Nature Biotechnology 2008 26:12. 2008;26: 1367–1372.
805 doi:10.1038/nbt.1511
806 47. Tyanova S, Temu T, Sinitcyn P, Carlson A, Hein MY, Geiger T, et al. The Perseus
807 computational platform for comprehensive analysis of (prote)omics data.
808 Nature Methods 2016 13:9. 2016;13: 731–740. doi:10.1038/nmeth.3901
809 48. Kawakami E, Watanabe T, Fujii K, Goto H, Watanabe S, Noda T, et al. Strand-
810 specific real-time RT-PCR for distinguishing influenza vRNA, cRNA, and mRNA. J
811 Virol Methods. 2011;173: 1. doi:10.1016/J.JVIROMET.2010.12.014
812 49. Courtney DG, Tsai K, Bogerd HP, Kennedy EM, Law BA, Emery A, et al.
813 Epitranscriptomic Addition of m5C to HIV-1 Transcripts Regulates Viral Gene
814 Expression. Cell Host Microbe. 2019;26: 217–227.
815 doi:10.1016/j.chom.2019.07.005
816 50. Choi JH, Luo J, Hesketh GG, Guo S, Pistofidis A, Ladak RJ, et al. Repression of
817 mRNA translation initiation by GIGYF1 via disrupting the eIF3-eIF4G1
818 interaction. Sci Adv. 2024;10: eadl5638. doi:10.1126/SCIADV.ADL5638
819 51. Broadbent L, Villenave R, Guo-Parke H, Douglas I, Shields MD, Power UF. In
820 Vitro Modeling of RSV Infection and Cytopathogenesis in Well-Differentiated

821 Human Primary Airway Epithelial Cells (WD-PAECs). Methods Mol Biol.
822 2016;1442: 119–139. doi:10.1007/978-1-4939-3687-8_9
823
824

825 **Supplementary data**

826 Supplementary Table 1 – Initial RIC dataset prior to downstream analysis

827 Supplementary Table 2 – RIC dataset of RBP identified in at least 2 replicates of each

828 condition, with fold enrichment and p values included.

829 Supplementary Table 3 – siRNA sequences

830 Supplementary Table 4 – Primer sequences

831 Supplementary Table 5 – Sequences of antisense oligonucleotides

832 Supplementary Table 6 – smiFISH probe sequences

833

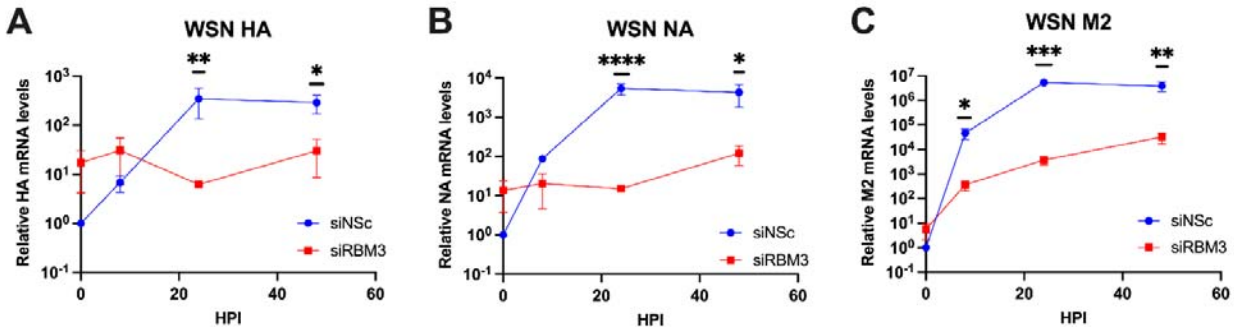

834

835 *Supplementary Figure 1 – IAV transcript levels upon loss of RBM3.*

836 *A549 cells were initially transfected with a negative control NSC siRNA or an RBM3-targeting siRNA and incubated for 48h.*
837 *RNA was harvested from these cells after infection with WSN at an MOI 0.01 and further incubation for 0, 8, 24 or 48 hpi.*
838 *Individual viral transcript levels were quantified by qPCR and normalised to GAPDH levels. Upon loss of RBM3 there was a*
839 *significant reduction in HA* ***(A)****, NA* ***(B)*** *and M2* ***(C)*** *mRNA levels, as determined by multiple t-tests. *=p<0.05, **=p<0.01,*
840 ****=p<0.001*

841

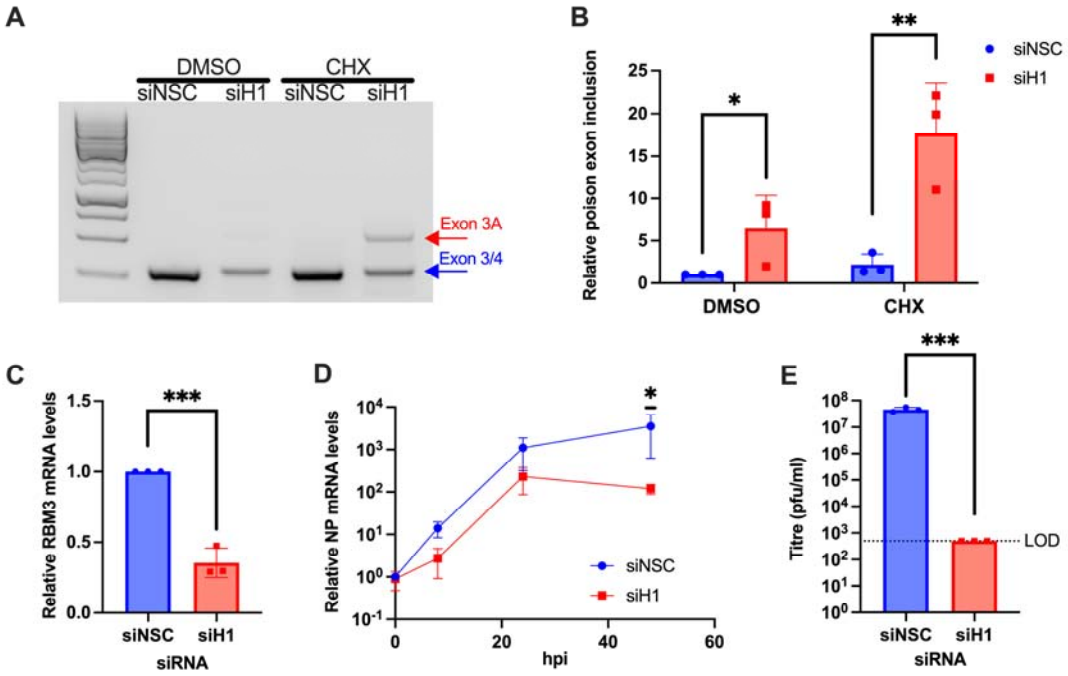

Supplementary Figure 2-Reduced RBM3 levels through manipulation of HNRNPH1 expression suppressed IAV replication

(A) *DNA gel showing inclusion of RBM3's poison exon, exon 3a. Cells were treated with siHNRNPH1 or siNSC and further treated 48 hours post-transfection with DMSO or CHX.* ***(B)*** *qPCR quantification of poison exon inclusion in the samples from Fig. 2D.* ***(C)*** *Quantification of RBM3 mRNA levels in siHNRNPH1 (siH1) A549 cells compared to siNSC treated cells.* ***(D)*** *Transcription levels of NP mRNA in siHNRNPH1 or siNSC treated A549 cells infected with WSN at 37°C.* ***(E)*** *Viral titres 72 hpi with WSN MOI 0.01 for siHNRNPH1 or siNSC treated cells.*

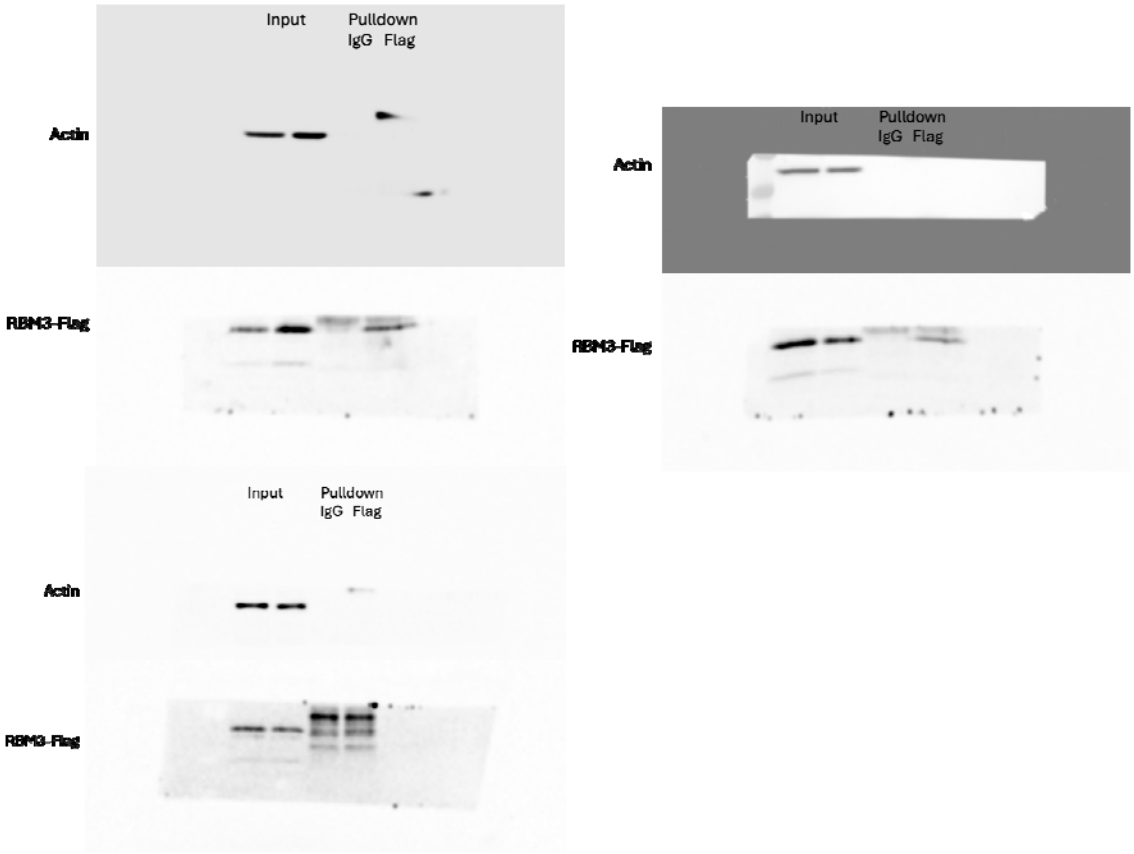

Supplementary Figure 3 – Western blot replicates for CLIP-qPCR in Figure 3E.

3 replicates of CLIP-qPCR experiments to pulldown RBM3-Flag in infected A549 cells demonstrating that RBM3-Flag is present in both input samples but only pulled down in the presence of Flag antibody, while Actin is not enriched in either pulldown sample.